Journal of Nuclear Materials 389 (2009) 443–449

Contents lists available at ScienceDirect

Journal of Nuclear Materials

journal homepage: www.elsevier.com/locate/jnucmat

Temperature and dose dependence of fission-gas-bubble swelling in U_3Si_2 ☆

Yeon Soo Kim [a,*], G.L. Hofman [a], J. Rest [a], A.B. Robinson [b]

[a] Argonne National Laboratory, Nuclear Engineering, 9700 South Cass Avenue, Argonne, IL 60439, United States
[b] Idaho National Laboratory, P.O. Box 1625, Idaho Falls, ID 83415-6188, United States

ARTICLE INFO

Article history:
Received 12 December 2008
Accepted 23 February 2009

ABSTRACT

Large fission gas bubbles were observed during metallographic examination of an irradiated U_3Si_2 dispersion fuel plate (U0R040) in the Advanced Test Reactor (ATR). The fuel temperature of this plate was higher than for most of the previous silicide-fuel tests where much smaller bubble growth was observed. The apparent conditions for the large bubble growth are high fission density (6.1×10^{21} f/cm^3) and high fuel temperature (life-average 160 °C). After analysis of PIE results of U0R040 and previous ANL test plates, a modification to the existing athermal bubble growth model appears to be necessary for high temperature application (above 130 °C). A detailed analysis was performed using a model for the irradiation-induced viscosity of binary alloys to explain the effect of the increased fuel temperature. Threshold curves are proposed in terms of fuel temperature and fission density above which formation and interconnection of bubbles larger than 5 μ are possible.

1. Introduction

Before the interest in developing U–Mo fuel prevailed, U_3Si_2 fuel received numerous tests both in-pile and out-of-pile as fuel for research and test reactors. As a result, a considerable literature has been accumulated [1–9]. U_3Si_2 is presently considered the best qualified fuel in terms of uranium loading and performance for these reactors. In U_3Si_2/Al dispersion fuel, interaction layers grow slower than in U–Mo/Al dispersions. The interaction layers (ILs) in U_3Si_2/Al are free of porosity formation, in contrast to U–Mo/Al. Fission gas bubbles in the unreacted fuel particles are generally small and stable except under extremely high burnup and/or high-temperature conditions.

In the past, fission gas bubble growth and fuel swelling has been considered athermal in the relatively low (<110 °C) temperature regime and dependent only on burnup [5,6]. Silicide compounds (U_3Si_2 and U_3Si) are known to become amorphous under irradiation [7,8]. Modeling work describing their irradiation behavior can be found in the literature (see for example Ref. [9], and references therein).

Recently, potential applications of this fuel to high-power research and test reactors rekindled an interest for additional tests [10–12]. The high-power reactor applications call for high heat fluxes (~260 W/cm^2), high burnups (~5×10^{21} fissions/cm^3), and high fuel temperatures (~140 °C). Although extensive data for the silicide fuel are available at Argonne National Laboratory (ANL) and in the literature, no data have been obtained at temperatures higher than 110 °C combined with high burnups. Some previous tests were at high temperatures, but the burnups were low [1,2].

In the RERTR-8 test [13] devoted mostly to U–Mo fuels, two U_3Si_2/Al dispersion fuel plates were included for normalization. The silicide fuel samples were irradiated under conditions similar to those for the U–Mo plates; these conditions in terms of temperature and fission density were much more severe than those seen by most of the silicide fuels tested previously. The silicide plate irradiated at the higher power position has been metallographically examined at the peak power location having fission density of 6.1×10^{21} f/cm^3 and life-average temperature of 160 °C. Metallography showed that the bubbles in this region are much larger than the maximum-size bubbles observed in prior tests. The large bubbles are distributed across all of the fuel particles seen in the optical micrographs. The maximum bubble size observed in the peak power region is ~40 μm. In addition, some of the large bubbles have begun to interconnect. It should be noted that the condition for fuel plate failure by breakaway swelling is the interconnection of fission gas bubbles throughout a significant area of the fuel meat.

2. Irradiation test

Two U_3Si_2/Al dispersion fuel plates were included in the RERTR-8 test. The U-loading was 4.7 gU/cm^3 of meat. The plate irradiated

☆ The submitted manuscript has been created by the UChicago Argonne, LCC as Operator of Argonne National Laboratory under Contract No. DE-AC-02-06CH11357 between the UChicago Argonne, LLC and the Department of Energy. The US Government retains for itself, and others acting on its behalf, a paid-up, nonexclusive, irrevocable worldwide license in said article to reproduce, prepare derivative works, distribute copies to the public, and perform publicly and display publicly, by or on behalf of the Government.

* Corresponding author. Tel.: +1 630 252 3173; fax: +1 630 252 5161.
E-mail address: yskim@anl.gov (Y.S. Kim).

0022-3115/$ - see front matter © 2009 Elsevier B.V. All rights reserved.
doi:10.1016/j.jnucmat.2009.02.037

at the higher-power location, C-6, in the test vehicle (U0R040) was metallographically examined. Plate U0R040 was irradiated for 104.7 effective full power days (EFPDs) with an average fission density of 4.7×10^{21} f/cm^3. The fuel enrichment was 74.9% U-235. The meat-average heat flux was 263 W/cm^2 at beginning of life (BOL) and decreased cycle-by-cycle to 177 W/cm^2 at end of life (EOL) [14].

Postirradiation gamma scans showed that substantial power peaks existed in the plate, not only transversely but also axially. This observation was also predicted by physics analyses [14]. The transverse power peaking occurs because the plate was loaded in the test vehicle with one side closer to the reactor core than the other side. The axial peaking is not as severe as the transverse peaking because the plate was irradiated in an axial location where the neutron flux is relatively flat. Whereas axial power peaking is negligible for LEU plates, it is considerable for highly enriched fuel such as U0R040.

In Fig. 1(a), the dots schematically show the points where the plate thickness data were obtained. In this paper, a thickness measurement point is written as (x,y) where x represents the transverse lines designated A–F and y represents the axial lines designated 1–3. The fission densities of U0R040 in the meat, calculated from the physics analysis data, are plotted in Fig. 1(b), where the thickness measurement points are also indicated.

A transverse section from the axial midplane of the meat, i.e., 2.5 mm below line D, was examined by optical metallography, as is the usual practice for RERTR test plates. However, as seen in the fission density map, the peak fission density occurs at the top corner of the plate near the measurement point $(F,3)$, where the heat flux is estimated to be ~363 W/cm^2. As discussed later, this location has a life-average temperature of 160 °C and a fission density of 6.1×10^{21} f/cm^3. Therefore, additional metallography was performed on a section cut along line 3 from the top of the meat to a point midway between $(E,3)$ and $(F,3)$.

3. Results

As shown in Fig. 2, postirradiation metallography of the transverse section of U0R040 at the axial midplane of the meat revealed smaller bubbles (~2 μm in diameter) on the cold side, i.e., near $(D,1)$ and large fission gas bubbles (~20 μm in diameter) on the hot side, i.e., near $(D,3)$. The bubble growth near $(D,1)$ is similar to that observed in the previous low-temperature tests.

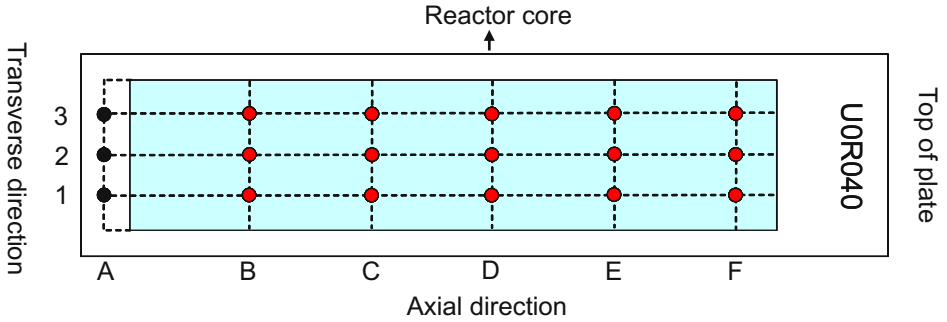

(a) Plate thickness measurement points. The meat axial midplane is located 2.5-mm off the line D toward the line C.

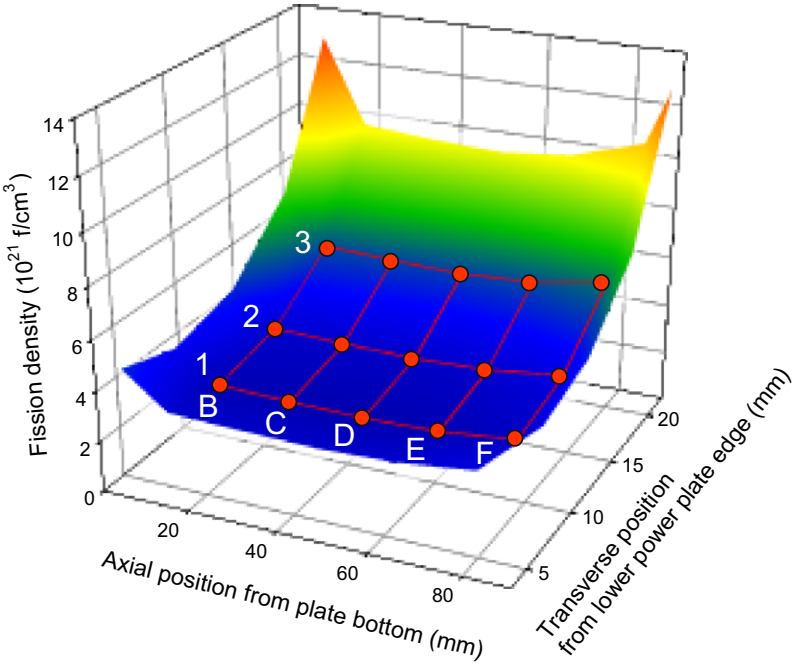

(b) Fission density map in fuel meat of U0R040.

Fig. 1. Plate thickness measurement points and fission density map of U0R040. The dots in (a) and (b) indiate the points where plate thicknesses were measured.

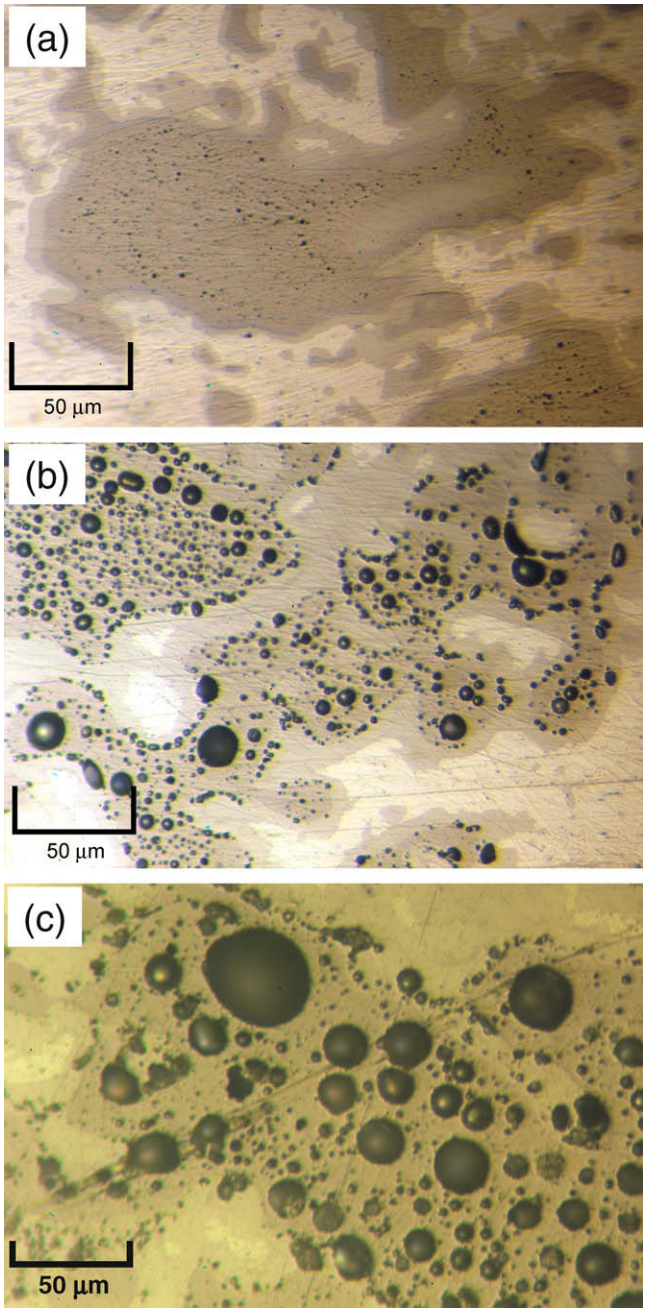

Fig. 2. Optical micrographs of U0R040 irradiated in ATR. (a) near $(D,1)$ where $T = 105$ °C and FD = 3.2×10^{21} f/cm^3; (b) near $(D,3)$ where $T = 136$ °C and FD = 5.4×10^{21} f/cm^3; (c) near $(F,3)$ where $T = 160$ °C and FD = 6.1×10^{21} f/cm^3.

The large gas bubbles near $(D,3)$ indicate unstable bubble growth that resulted in high fuel swelling. The growth of abnormally large bubbles is caused by interconnection of small bubbles that can result in fuel failure by pillowing. The bubble size measured at $(F,3)$ is ~40 μm. The interaction between the fuel and matrix is so great that only a tiny bit of the Al matrix remains. Some of the large bubbles are starting to interconnect, which is a preliminary step for pillowing.

A lower magnification micrograph, not included here, shows that large bubbles are present throughout the fuel meat cross section, but some fuel particles generally have smaller bubbles than nearby particles. However, the extent of bubble growth is similar to that of U_3Si from previous tests, which is known to have significantly larger bubble growth than U_3Si_2.

Fuel temperatures are calculated by using the IL growth correlation developed for U_3Si_2/Al dispersion fuel at ANL [1,15]:

$$Y = [2.2 \times 10^{-8} \exp(-4882/T)\dot{f}^{0.5} t]^{0.5}, \quad (1)$$

where Y = interaction layer thickness (μm), T = life-average fuel meat temperature (K), $\dot{f}$ = fission rate (fission/cm^3 s), and t = irradiation time (s). Rearranging Eq. (1) for T gives:

$$T = \frac{4882}{\ln(2.2 \times 10^{-8} \dot{f}^{0.5} t / Y^2)}. \quad (2)$$

Using Eq. (2), T can be calculated for a test plate with known $\dot{f}$, t and IL thickness.

The results of the analysis of U0R040 data are given in Table 1. The test data available in the literature and by private communication, as well as previous ANL in-house data, are also included in the table. In this paper, fission rates and densities include not only fissions of U-235 but also those of Pu atoms generated during irradiation. When the temperatures were not known, the life-average fission rate, measured IL thickness, and irradiation time were used in Eq. (2) to calculate the life-average fuel temperature. The JMTR [2] and HFIR [1] tests had nearly constant temperatures during the test, whereas all other tests had changing temperatures over the irradiation period. The temperatures of the JMTR and HFIR tests were confirmed by comparing with the calculated values using Eq. (2).

The uncertainties in fission density (FD) and fission rate (FR) are small (less than 5%). The uncertainties in calculated temperatures are due mostly to errors involved in IL thickness measurements. The temperature obtained by using Eq. (2) is dependent upon the postirradiation IL thickness and is thus the life-average number. The temperature of a test plate usually changes during irradiation, as is the case for U0R040. Fig. 3 shows a comparison between the IL thickness prediction made with Eq. (2) using variable temperature and FR histories of U0R040 with the measured IL thickness. The difference is ~0.1 μm, which corresponds to life-average temperature of less than 1 °C. Fig. 3 also shows the sensitivity of IL thickness on temperature obtained using Eq. (2). An increase in the end-of-life IL thickness by 0.25 μm (or 4% of total thickness) obtained by keeping the FR unchanged yields 3 °C higher temperature. Because the error in IL thickness measurement is typically less than 0.25 μm, the uncertainty related to the temperature estimation method is

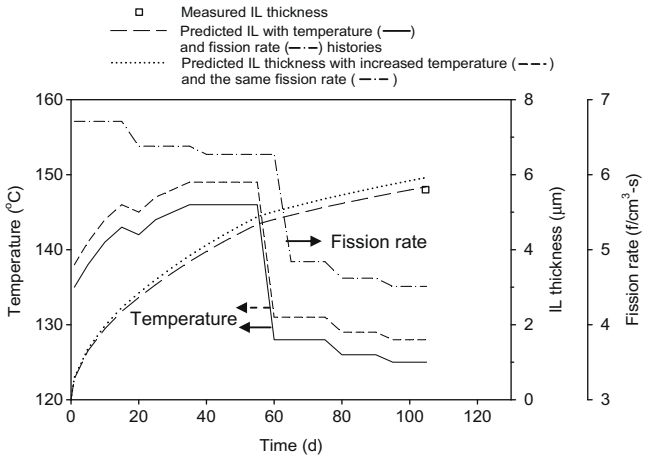

Fig. 3. Comparison of predicted IL thickness (shown by long dash) using temperature and fission rate histories with measured IL thickness for U0R040 near $(D,3)$. An increase in temperature by 3 °C (shown by the broken line) yields 0.25 μm increase in the end-of-life IL thickness (shown by the dotted line).

Table 1
Summary of irradiation data of U_3Si_2/Al.

Test reactor (sample ID)	Enrichment	Time EFPD	FR♣ 10^{14} f/cm^3 s	FD★ 10^{21} f/cm^3	T♣ (°C)	IL (μm)	Bubble size (μm)†	Inter-connected bubbles	Data source
BR-2 (first test)	35			1.3	240		<1	No	[10]
JMTR (88F-01)	19.8	108	1.8	1.7	200	10.0	2	No	[2]
ATR (R5-U6008J)	19.5	116	1.9	1.9	109	3.0	0.6	No	✧
ATR (R1-W002)*	19.5	94	2.6	2.1	65	1.0	0.4	No	✧
ORR (A100)	19.8	174	1.4	2.1	90	2.0	0.6	No	✧
HANARO (KOMO-3)⌖	19.5	206	1.4	2.5	142	6.0	3	No	[16]
ATR (R8-U0R040)^C	74.9	105	3.5	3.2	105	3.0	2	No	♦
ATR (R2-W003)	19.5	232	1.8	3.6	65	2.0	0.6	No	✧
ORR (A99)	19.8	385	1.3	4.2	100	4.0	1	No	✧
FRJ-2 (test 1–#10)	19.7	321	1.4	4.0	130	6.0	6	No	[3]
BR-2 (second test)	19.9	69	8.1	4.8	135	4.8	3	No	[11]
HFIR (HANS 3–10)	19.8	23	25.0	5.0	220	10.0	6	Yes	✧
ATR (R8-U0R040)^H	74.9	105	5.7	5.4	136	5.6	20	No §	♦
NRU (FL-050 center)⌖	19.7	238	2.8	5.7	137	7.0	6	No	[4]
ATR (R8-U0R040)^P	74.9	105	6.7	6.1	160	8.2	38	Yes	♦
ORR (A121)	92.6	130	8.4	9.4	100	3.2	3	No	✧
ORR (A122)	92.6	272	6.1	14.3	100	4.4	15	No	✧

♣The fission rate and temperature are the life-averaged values. ★ Fission density is for fuel particles. † Diameter of maximum-size bubble; threshold size for an unstable bubble is tentatively set at 5 μm. ✧ Data obtained in previous ANL tests and reanalyzed in the present study. ♦ Data obtained in the present study. * R is an abbreviation of RERTR such that, for example, R1 means the RERTR-1 test. § Some bubbles show the initial stage of interconnection. ⌖ HANARO and NRU data are for rod-type fuel, all other data are for plate-type fuel. C = near $(D,1)$, H = near $(D,3)$, P = near $(F,3)$ points in Fig. 1(a).

considered smaller than 3 °C. The sensitivity of the FR on temperature obtained by using Eq. (2) is even smaller than the sensitivity of IL thickness on temperature. Although not shown in Fig. 3, a 10% error in the FR over the entire life yields only a degree difference in temperature.

4. Discussion of postirradiation results

A plot of fuel temperature versus FD for the previous tests and for the recent U0R040 test is shown in Fig. 4. After studying all of the available data, a bubble size of 5-μm diameter appears to be a reasonable threshold for characterizing bubbles as being 'large.' Samples containing large bubbles are designated by colored symbols. Previous observations have shown that bubbles were smaller than ~1 μm for most tests at low temperatures (<110 °C). The data shown by red symbols are for those with interconnected bubbles. A combination of sufficiently high fuel temperature and sufficiently high FD appears to be necessary for the formation of large bubbles, some of which can become interconnected. Two tentative threshold curves are shown in the figure: one for large bubble formation and the other for interconnected large bubble formation. The FD asymptotically decreases to a threshold value as the temperature increases because a minimum FD is required before large fission gas bubbles can form. On the other hand, the threshold temperature gradually decreases as the FD increases.

The thresholds are shown as shaded areas, indicating considerable uncertainty owing to the sparseness of the dataset. For example, the test results from the second BR-2 test and the FRJ-2 test are on the threshold for large bubble formation. The FRJ-2 test plate contained 6-μm bubbles uniformly distributed in the fuel particles, and the BR-2 test plate contained 3-μm bubbles, although the former has a lower FD than the latter. The BR-2 test plate also contained maximum 21-μm-size bubbles in localized U_3Si phases within the U_3Si_2 fuel particles [11]. Bubble growth is faster in U_3Si than in U_3Si_2. For most of the test samples, however, the local phase inhomogeneity in the fuel particles where the micrographs were taken is unknown. Therefore, it is uncertain whether the large bubbles are indeed included in U_3Si_2.

One of the most important variables in the performance of U_3Si_2 is the existence of the so-called secondary phases, viz., U solid solution, U_3Si, or USi. These phases have different gas bubble swelling and interaction layer growth kinetics than U_3Si_2. In general, as the Si/U ratio increases, both bubble growth and IL growth rates decrease. However, it is essentially impossible to produce pure U_3Si_2 at the exact stoichiometric composition. The practice at ANL has been to make slightly Si-rich alloys that lead to final products containing the secondary phases with the maximum amounts of 3 vol.% of U solid solution, 10 vol.% of U_3Si, or 15 vol.% of USi [5]. The secondary phases typically reside inhomogeneously in a fuel particle so that the size of fission gas bubbles varies within a fuel particle, as well as from particle to particle. The postirradiation microstructure of U0R040 also shows this inhomogeneity.

As FD increases, the Si/U ratio of the fuel increases. The question is whether the fuel becomes more stable and, therefore, experiences even slower bubble growth. Comparison of the A-121 and A-122 data in Fig. 4 rejects this possibility. A-122, with a higher FD than A-121, shows large bubble growth while A-121 does not. A possible explanation can be found in the fission product yield. The transition metal elements and rare earth elements are produced at a rate of ~1.3 atoms per fission. Therefore, the increase in the concentrations of fission products is larger than the decrease in the U concentration. Some of the fission products, for example Zr, have higher affinity for Si than U, ultimately reducing the effective Si/U ratio.

A temperature effect can be seen if a comparison is made between the behaviors of W003 from ATR, A-99 from ORR, and Plate #10 from FRJ-2 (see Table 1). These test samples have similar FDs, having been irradiated for long times, but the fuel meat temperatures were different. However, only the FRJ-2 sample, which had the highest temperature of the three samples, contains much larger bubbles than the others. Except for the extremely high FD test of A-122 in ORR, bubbles larger than 5-μm were only observed at fuel meat temperatures higher than 130 °C.

Fig. 5 is a micrograph showing bubble morphology of U_3Si irradiated at 100 °C to a FD of 5.3×10^{21} f/cm^3 in ORR. The bubble morphology is indistinguishable from that of high-temperature U0R040 shown in Fig. 2(c). This shows that bubble growth in U_3Si_2 can be enhanced to the level of U_3Si if the temperature is increased. U_3Si_2 appears to experience a bubble growth phenomenon at high temperatures similar to that of U_3Si at low temperatures – the low bubble growth advantage of U_3Si_2 provided by the high Si/U ratio is negated by increasing the temperature. A theoretical explanation of the temperature effect is given in Section 5.

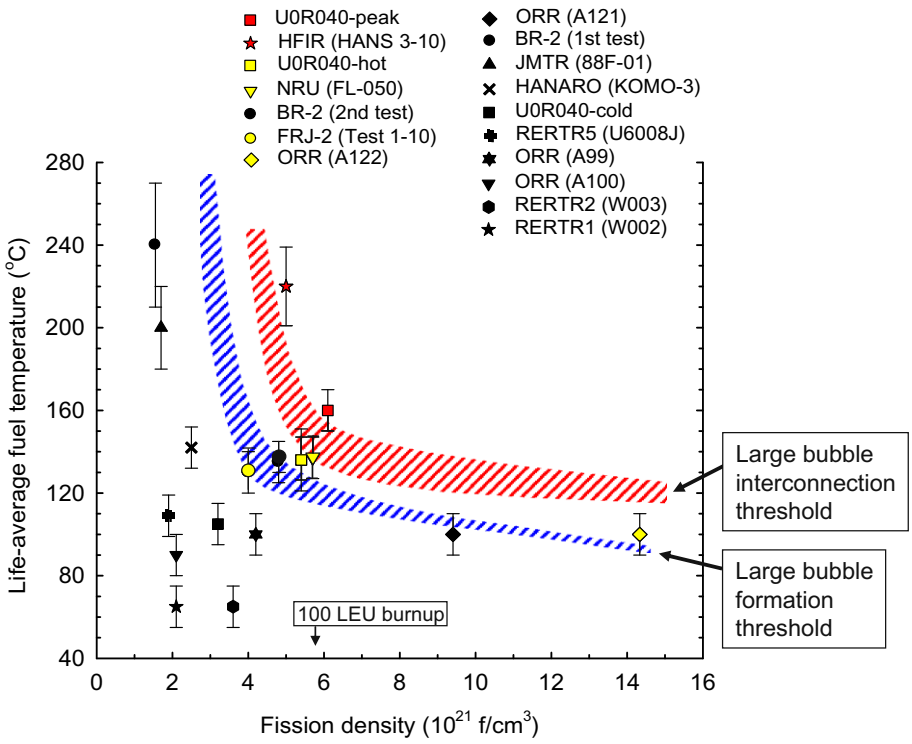

Fig. 4. Estimated fission density–temperature thresholds for large bubble formation (greater than 5 μm) and for interconnected gas bubble formation in U_3Si_2. The shaded areas indicate the uncertainties in the thresholds.

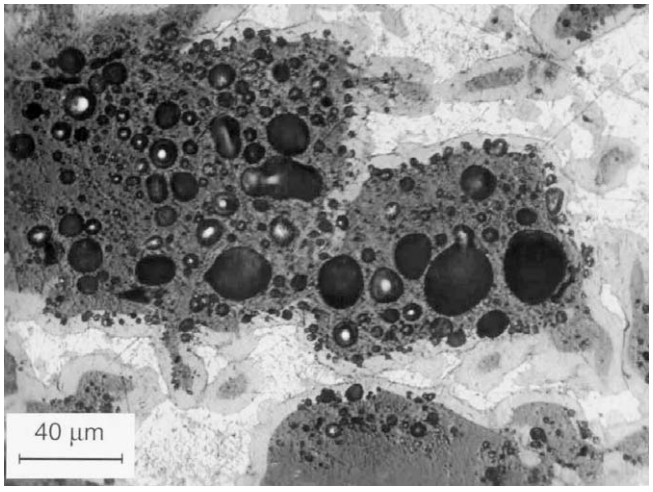

Fig. 5. Optical micrograph of U_3Si-Al irradiated for 319 days to fission density of 5.3×10^{21} f/cm^3 at life-average temperature of 100 °C in ORR (A105 plate).

5. Theoretical interpretation of bubble growth

A large number and variety of compounds and alloys have been found to become amorphous when exposed to various types of irradiation [17]. For nuclear fuels, the primary damage to the crystal structure is due to the highly energetic fission fragments. Amorphization is a low temperature phenomenon and amorphized materials recrystallize at the so-called critical temperature. Above this temperature, amorphization is not possible and the fuel exhibits crystalline irradiation behavior. Fuel behavior can be quite different in amorphized fuels. Diffraction studies have revealed that both U_3Si and U_3Si_2 become amorphous almost instantly under irradiation [7,8]. Fig. 4 shows the fission gas bubble morphology in irradiated U_3Si [17]. This fuel developed very large bubbles that led to unacceptable breakaway swelling. The extremely high growth rate of fission gas bubbles in U_3Si was attributed to fission-induced amorphization [18]. Such a transformation resulted in changes in fission gas mobility and the plastic flow rate of the fuel that were responsible for the swelling increases. Postirradiation hardness tests showed that this fuel had retained its relatively hard and brittle pre-irradiation property. The observed fluid-like behavior thus only exists during irradiation. Klaumunzer [19] has demonstrated this irradiation behavior with heavy ion beam irradiations of borosilicate glasses and Pd-Si metallic glasses. He was able to correlate the measured increase in fluidity in these tests with the excess free volume that was independently measured on these glasses.

As shown in Fig. 2(a), this extreme behavior was not observed in the lower density compound U_3Si_2 irradiated at 105 °C, where a distribution of relatively small and stable fission gas bubbles was observed to form and remain throughout the irradiation to very high burnup [6]. A mechanistic rate-theory model developed by one of the authors (Rest) to interpret the behavior of fission gas in irradiated amorphous materials such as U_3Si and U_3Si_2 demonstrated that the bubble coarsening process depends on the materials viscosity [9]. Estimated irradiation-induced viscosity values were obtained by comparing the calculated bubble-size distribution with the observed average bubble size and density as a function of fission rate and burnup. In addition, the analysis demonstrated that the estimated irradiation-induced viscosity of a U–Si compound is a strong function of the composition. Based on the results of this work, a new theoretical model was developed recently [20] to calculate the viscosity of binary alloys as a function of composition. This model predicts the viscosity values determined from the bubble-size distribution analysis. This model is used in this paper in order to provide an estimate of the effect of temperature on the irradiation-induced viscosity of U_3Si_2. Thus, in order to utilize such models in a quantitative fashion (e.g., to

calculate gas-bubble driven swelling), a quantitative estimate of the materials viscosity as a function of composition and irradiation conditions is required.

For the case of irradiation-induced amorphization, the Adam–Gibbs relation [21] for the intrinsic viscosity η is expressed as:

$$\eta = \eta_0 \exp\left[\frac{A}{S_c T}\right], \tag{3}$$

where S_c is the configurational entropy, η_0 and A are constants, and T is the absolute temperature.

In order to determine S_c in Eq. (3), the entropy of mixing of solid alloys is calculated using a generalized hard sphere model of binary fluids in an application to alloys that undergo an irradiation-induced crystalline–amorphous transformation [20]. The basic assumption here is that the behavior of certain irradiated amorphous materials is 'liquid like.' This model, in simple form, views each alloy component, before mixing, as a collection of hard spheres of suitable diameter; then, on mixing, the hard sphere diameters are adjusted such that the mean volume per atom of the alloy is recovered.

The connection between a real liquid metal and a hard sphere liquid is provided by the attractive forces of the real particles which give rise to cohesion of the real liquid. A generalization of the model due to such attractive forces is obtained by adding the effect of a uniform negative background potential to the hard sphere model.

The amorphization of crystalline alloys under irradiation proceeds in solid state and is mainly driven by the kinetic energy implanted through irradiation, which is currently believed to result either from accumulation of a critical density of point defects, anti-sites (as in SiC), or some combination. This is significantly different from the amorphization of equilibrium liquids by rapid quenching, or even the solid amorphization by mechanical alloying, in terms of the direction of the thermodynamic transitions. The kinetics of amorphization and swelling under irradiation are related to the irradiation conditions as closely as, if not more so than, to the alloy's intrinsic (without irradiation) behavior such as equilibrium viscosity. In this context, irradiation acts as the crystalline to amorphous transformation mechanism. That various amorphous materials behave in a liquid-like fashion under irradiation is supported by a large body of literature (e.g., see Refs. [19,22], and references therein). In the end, the assumptions incorporated in this work are justified, or contradicted, by comparison of the models predictions with experiment.

Work on ion-beam induced plastic deformation of amorphous solids has revealed that for these conditions the viscosity is inversely proportional to the strain rate [19,22]. Here, the irradiation-induced viscosity η_I is assumed to have a similar dependence on fission rate as it has on strain rate, i.e. the viscosity is inversely proportional to the fission rate $\dot{f}$,

$$\eta_I = \eta \dot{f}_0 / \dot{f} \tag{4}$$

where, in general, η is given by Eq. (3), and $\dot{f}_0$ is the minimum fission rate for which the material will remain amorphous. The validity of Eq. (4) is supported by observations of plastic flow of insulating glasses, amorphous semiconductors, and glassy metals [19]. In addition, this same dependence was derived in a thermal spike model for irradiation creep of amorphous solids which compared well with experimental data for ion irradiated vitreous silica [23]. The basis for this behavior is described by Trinkaus and Ryazanov [24] as anisotropic growth of amorphous materials subject to intense electronic excitations resulting from the efficient relaxation of shear stresses within cylindrical thermal spike regions induced by the thermal dilatation and to the subsequent freezing-in of the associated shear strain increments.

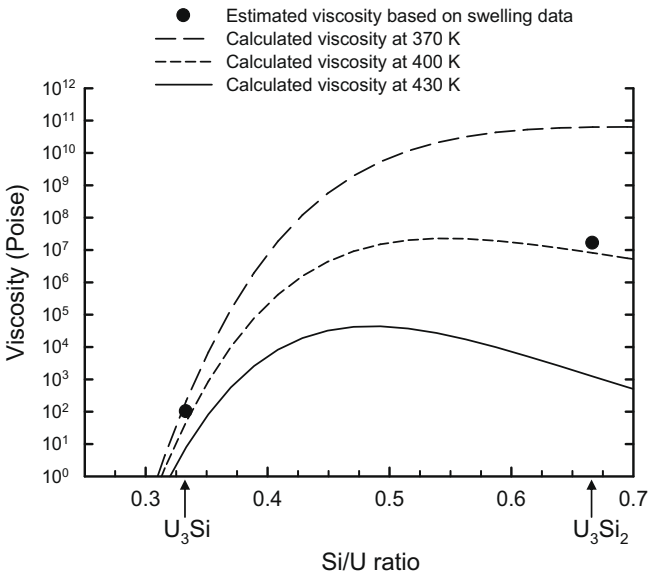

Fig. 6. Viscosity versus Si/U ratio for three temperatures.

As shown in Fig. 6, the generalized hard sphere model was used to calculate the viscosity of U–Si as a function of Si/U ratio for three values of the irradiation temperature. The calculated temperature dependence of the viscosity is dependent on an assumption made in the analysis that the rate of change of the calculated formation enthalpy with respect to temperature is symmetric about the uranium concentration corresponding to the curve minimum. In addition, the temperature independence of certain materials properties (such as thermal expansion coefficient) has also been assumed. Thus, only the trend of the calculations should be considered at this time. It is important to note that as U_3Si_2 is irradiated, the Si/U ratio shifts to the right. In any event, the calculations show that an ~30 K increase in temperature results in a viscosity for U_3Si_2 that is similar to that of U_3Si irradiated at the lower temperature. In addition the calculated viscosity of U_3Si_2 is much more sensitive to temperature than that of U_3Si.

6. Conclusion

U0R040 (a U_3Si_2 plate) irradiated as part of the RERTR-8 test was examined. U_3Si_2 showed abnormally large fission gas bubbles. A maximum bubble size of ~40 μm was observed at a fuel life-average temperature of 160 °C and a fission density of 6.1×10^{21} f/cm^3. The bubble morphology is similar to that of U_3Si irradiated at low-temperature (<110 °C) and low fission density. At high temperature (130 °C < T), the thermal contribution to U_3Si_2 gas bubble growth is considerable.

The interconnected large bubble growth yielded fuel swelling of ~90%, which is greater than U–Mo fuel swelling at the same fission density and temperature. Fuel temperature and fission density are identified as two determining factors for large bubble growth and interconnection of large bubbles. A threshold is proposed in terms of life-average temperature and fission density above which formation of bubbles larger than 5 μm is possible. Another threshold is also proposed in terms of fuel temperature and fission density above which interconnection of large bubbles (>5 μm) can occur.

Models developed at ANL were used to interpret the behavior of fission gas in irradiated amorphous materials such as U_3Si_2 and U_3Si, in which the bubble coarsening process depends on the material's viscosity. The model predictions showed that an ~30 K

increase in temperature reduces the viscosity of U_3Si_2 to a level that is similar to that of U_3Si irradiated at a much lower temperature, which follows the trend of the observed bubble growth in U0R040. The model also predicts that the gas bubble growth of U_3Si_2 is much more sensitive to temperature than that of U_3Si because the former has a more temperature-sensitive viscosity than the latter.

Acknowledgments

The authors are grateful to Dr J.L. Snelgrove for his careful review of the paper and comments. The authors would like to thank Dr D.M. Wachs for the RERTR-8 test. PIE work at the MFC-INL is also appreciated.

References

[1] G.L. Hofman, J. Rest, J.L. Snelgrove, T. Wiencek, S. Koster van Groos, in: Proceedings of International Meeting Reduced Enrichment for Research and Test Reactors, 7–10 October 1996. Available from: <http://www.rertr.anl.gov/index.html>.
[2] M. Ugajin, M. Akabori, A. Itoh, H. Someya, T. Nakagawa, K. Ohsawa, in: Proceedings of International Meeting Reduced Enrichment for Research and Test Reactors, JAERI-M-94-042, 1993.
[3] W. Krug, E. Groos, J. Seferiadis, G. Thamm, ANL/RERTR/TM-13 CONF-8809221, in: Proceedings of International Meeting Reduced Enrichment for Research and Test Reactors, 19–22 September 1988, Argonne National Laboratory, 1988.
[4] D. Sears, M.F. Primeau, C. Buchanan, D. Rose, in: Proceedings of International Meeting Reduced Enrichment for Research and Test Reactors, 18–23 September 1994, ANL/RERTR/TM-20 CONF-9409107, Argonne National Laboratory, 1994.
[5] J.L. Snelgrove, R.F. Domagala, G.L. Hofman, T.C. Wiencek, G.L. Copland, R.W. Hobbs, R.L. Senn, Argonne National Laboratory, Report ANL/RERTR/TM-11, 1987; also in Safety Evaluation Report, NUREG-1313, 1988.
[6] M.R. Finlay, G.L. Hofman, J.L. Snelgrove, J. Nucl. Mater. 325 (2004) 118.
[7] R.C. Birtcher, J.W. Richardson, M.H. Mueller, J. Nucl. Mater. 230 (1996) 158.
[8] R.C. Birtcher, J.W. Richardson, M.H. Mueller, J. Nucl. Mater. 244 (1997) 251.
[9] J. Rest, J. Nucl. Mater. 325 (2004) 107.
[10] A. Leenaers, S. Van den Berghe, E. Koonen, P. Jacquet, C. Jarousse, B. Guigon, A. Ballagny, L. Sannen, J. Nucl. Mater. 327 (2004) 121.
[11] A. Leenaers, E. Koonen, Y. Parthoens, P. Lemoine, S. Van den Berghe, J. Nucl. Mater. 375 (2008) 243.
[12] G.L. Hofman, Yeon Soo Kim, J.L. Snelgrove, RERTR Annual Report, Argonne National Laboratory, 2005.
[13] G.L. Hofman, Yeon Soo Kim, J. Rest, A.B. Robinson, D.M. Wachs, Trans. RRFM 2008, 2–5 March 2008, European Nuclear Society, 2008. Available from: <http://www.rrfm2008.org>.
[14] M.A. Lillo, G.S. Chang, Idaho National Laboratory, 2008 (unpublished information).
[15] Yeon Soo Kim, G.L. Hofman, Argonne National Laboratory, 2008 (unpublished information).
[16] H.J. Ryu, J.M. Park, C.K. Kim, private communication, KAERI, 2008.
[17] G.L. Hofman, Yeon Soo Kim, Nucl. Eng. Tech. 37 (2005) 299.
[18] J. Rest, G.L. Hofman, R.C. Birtcher, in: N.H. Packen, R.E. Stoller, A.S. Kumar, (Eds.), Proceedings of Effects of Radiation on Materials, 14th International Symposium, vol. II, ASTM STP 1046, Am. Soc. Test. Mater., Philadelphia, 1990, p. 789.
[19] S. Klaumunzer, Rad. Eff. Defects Solid 110 (1989) 79.
[20] J. Rest, Comput. Mater. Sci. 44 (2008) 207.
[21] G. Adam, J.H. Gibbs, J. Chem. Phys. 43 (1965) 139.
[22] S.S. Klaumunzer, C. Li, S. Loffler, M. Rammensee, G. Schumacher, H.Ch. Neitzer, Rad. Eff. Defects Solids 108 (1989) 131.
[23] H. Trinkaus, J. Nucl. Mater. 246 (1997) 244.
[24] H. Trinkaus, A.I. Ryazanov, Phys. Rev. Lett. 74 (1995) 5072.